# Towards Prediction of Failure in Ti-6Al-4V Aerospace Materials by Surface Observations

Theodore E. Matikas

Materials Engineering Department, University of Ioannina, University Campus, 45110 Ioannina, Greece

**ABSTRACT:** This paper deals with the development of a methodology for the prediction of material failure in metallic aerospace alloys by evaluating changes in surface characteristics directly prior to unstable fatigue crack propagation. The study is based on *in situ* nondestructive characterisation of the depression zone ahead of the crack tip of fatigue-pre-cracked titanium alloy specimens subjected to static loading. A relationship between the surface characteristics of the deformation zone ahead of the crack and the stress intensity factor of the material was obtained. This relationship was common to a variety of microstructural conditions such as mill-annealed and $\beta$-annealed microstructures. Based on the analysis, prediction of the impending fracture in cracked samples of the material was enabled. The outcome of this study can be used for optimising the service life of structural components.

**KEY WORDS:** *fatigue failure, surface characterisation, titanium alloys*

## Introduction

Extending the life of ageing aircraft beyond their design life requires knowledge of the fractional life remaining in the materials of key aircraft components. In this effort, nondestructive testing of critical components and application of fatigue crack damage-tolerance approaches are essential for predicting the residual life of key components containing measurable flaws. Current damage models used to determine the remaining life of components are, however, extremely conservative [1]. The conservative approach, known as 'fail-safe' standards, not only prevents failures but also leads to a lower level of component utilisation or more frequent and costly inspection. More efficient criteria for predicting fatigue crack failure and optimising service life of ageing aircraft may arise from recognising the changes in material properties directly prior to unstable crack growth. Quantification of the deformation zone at a crack front may enable prediction of fatigue crack instability, which leads to component failure [2–4]. This additional knowledge would allow application of a 'predict and manage' philosophy to maintaining aircraft, rather than the current and less efficient 'find it and fix it' maintenance approach.

The objective of this study was to develop a method for internal damage assessment and residual life prediction in aerospace materials and components by nondestructive evaluation of changing surface characteristics because of cracking. The material surface characteristics under observation include the tip of a fatigue crack and the plastic and elastic zones preceding it.

Titanium alloy specimens were used in this study, as high-performance aerospace components are often made of titanium-based materials. Prominent components made of titanium alloys include aircraft fuselage, gas turbine engine discs and blades, landing gears, lower wing skins and windshield frames [5]. Many of these are key structural components that require high-strength and damage-resistant alloys. Surface and subsurface damage in fracture-resistant aerospace structural materials such as titanium alloys can be due to fatigue, corrosion, foreign object impact and fretting. Subsurface damage caused by fatigue may be detected on the surface of polished samples through surface deformation or slip-band formation in locations where the cracks reach the surface [6]. It is widely believed that this deformation zone preceding a crack increases the effective length of the crack and, therefore, should be considered in life prediction models [7]. The presence of an effective crack length makes it necessary to develop methods to characterise and quantify subsurface damage and plastic deformation through characterisation of the surface, which is the most convenient location for crack-tip observations. The deformation is a result of complex stresses and strains at the crack tip. The presence of these stresses and strains is

 

exemplified by necking of the material. The localised necking creates a depressed volume in front of the crack tip. When the stresses and strains in the deformation area combine to reach a critical level, the conditions for crack propagation are satisfied. The crack extends through microcrack coalescence or increased necking, which causes voids to grow larger [7]. Through the conditions of its existence, the deformation zone can be considered to measure the load history of the material ahead of the crack following its last propagation step. The deformation zone is a combination of elastic and plastic deformations. The elastic deformation can be recovered while the plastic deformation, caused by a stress concentration at the crack tip that exceeds the material's yield strength, is permanent. Both mill-annealed and $\beta$-annealed titanium alloys were studied. White-light interference profilometry was used in both cases for *in situ* topographical data acquisition.

## Fracture Mechanics Approach and Crack-Tip Deformation

The Griffith theory can reasonably predict the onset of rapid fracture in somewhat brittle materials, but fails when applied to ductile materials that experience plastic deformation. In ductile materials, stress states and energy at the crack tip differ greatly from the conditions predicted by Griffith. These differences can be related to the amount of plastic deformation present at the point of fracture of a ductile material. Plastic deformation represents absorbed energy. This absorbed energy creates microscopic shear fracture surfaces instead of directly contributing to crack propagation [8]. The Griffith theory is based on the assumption that crack propagation occurs when an amount of energy exceeding that required for an increment of crack advance is absorbed. When plastic deformation is large in comparison with the crack length, standard fracture mechanics does not reasonably predict material failure because it fails to account for the energy absorbed by plastic deformation [8]. The stress intensity factor, $K$, describes the stress state of a defect within a component. The magnitude of the stress intensity factor changes based on the amount of damage preceding a crack. Accurate determination of the stress intensity factor for cracks with large deformation is difficult. Difficulties arise when the deformation field data extend into areas of the material influenced by the geometry of the specimen. It is also difficult to ensure that the surface deformations are representative of the displacements occurring throughout the sample bulk. This is guaranteed by taking measurements outside of the area one half of the plate thickness away from the crack tip [9].

## Need for New Surface Characterisation Tools to Quantify Crack-Tip Deformation

Numerous optical examinations of crack-tip deformations have been performed to estimate the stress state of a crack tip. These techniques include photoelastic methods [10], moiré interferometry [11–15], electronic speckle pattern interferometry [16], holographic interferometry [17], shearing interferometry [18], computer vision [19], caustics and numerical analyses [20], and full-field optical methods [21, 22]. Despite the importance of optical stress-analysis methods in fracture mechanics, there is a lack of suitable experimental techniques providing full-field deformation measurement [23]. In addition, all these methods have important limitations. For instance, photoelasticity requires calibration of each batch of material tested at the time of testing and is limited to specific materials. Moiré interferometry requires extensive surface preparation as a physical grating must be applied to the specimen surface prior to examination. Holographic and speckle interferometries require two exposures of the specimen surface on the same film, one reference exposure prior to deformation and another exposure following deformation.

To overcome the difficulties of traditional optical techniques, white-light interference profilometry was used in this study for acquisition of deformation field data. White-light interference profilometry measures the same physical properties as other optical methods, but it produces more interpretable topographical images as it enables non-contact, full-field, real-time, high-resolution 3-D evaluation of surfaces [24]. A white light interference profilometer is essentially a Michelson interferometer with a reference mirror replaced by the surface to be imaged [25–27] and can evaluate surfaces with a roughness as high as 500 $\mu$m, with 3 nm vertical resolution and lateral surface resolution of up to 0.2 $\mu$m. Such precision permits detailed topographic imaging. In addition, the technique is time-effective as imaging cycle time for medium-resolution scans up to 1 mm$^2$ in size is less than 5 min. Short scanning times enable *in situ* measurements such as the time-dependent measurements of crack front deformation performed in this study.

  

## Surface Characteristics of Crack-Tip Deformation

The deformation observed on the surface of a sample is a combination of elastic and plastic deformation. To distinguish the two types of deformation, a technique other than white-light profilometry must be applied. Standard techniques that identify plastic deformation include isochromatic-fringe experiments, photoelastic coating methods, etch-pit techniques, electrolytic etching, microhardness methods, electron channelling, X-ray diffraction, channelling contrast in scanning electron microscopy and stereographic techniques [7].

Assuming that elastic deformation is negligible, the size of the deformation zone can be estimated using standard fracture mechanics equations that calculate the radius, $r_y$, of plastic deformation,

$$r_y = \frac{K^2}{n\pi\sigma_{yx}^2} \tag{1}$$

with $n = 6$ for plane strain conditions and $n = 2$ for plane stress conditions; where $\sigma_{yx}$ is the yield stress in the loading direction and $K$ is the stress intensity factor.

Equation (1) is valid for applications where monotonic stress is present. When cyclic stresses are applied, the size of the plastic zone is greatly reduced. The cyclic deformation zone is estimated to be one-fifth the size of a monotonically loaded deformation zone [7]. A plane stress equation is used for plastic deformation radius equations in this study. The plane stress condition is valid for this study both because of the thickness of the samples and the comparison of plastic deformation calculations with surface deformation measurements. First of all, the samples were thin enough for the plane stress state to exist throughout the thickness of the sample. Secondly, this study is based on deformation measurements on the surface of the sample where the plane stress state is guaranteed to be present, regardless of the sample thickness, due to the lack of the 3-D stress state on the sample surface.

The shape of the plastic zone also affects the life of structural components. Equation (1) simply supplies the average radius of the plastic zone. Theoretical plastic zone shapes are not circular so an angular dependent radius of plastic deformation equation is needed, as shown in Equation (2):

$$r_y = \frac{K^2}{2\pi\sigma_{yx}^2}\cos^2\frac{\theta}{2}\left(1 + 3\sin^2\frac{\theta}{2}\right) \tag{2}$$

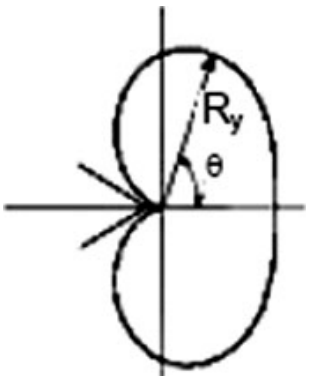


**Figure 1:** Shape of theoretical plastic deformation

Plotting this radius provides the theoretical plastic deformation shape for plane stress conditions of a crack at a particular stress intensity value [12]. This theoretical shape resembles a butterfly as seen in Figure 1.

## Materials and Testing

Both mill-annealed and $\beta$-annealed Ti-6Al-4V alloys were studied. Ti-6Al-4V cross-rolled sheet material 1.35 mm thick, annealed at 700 °C, was used in this study. The mill-annealed microstructure had grain sizes of approximately 5 $\mu$m in the transverse direction and 20 $\mu$m in the longitudinal direction. The $\beta$-annealed sheet examined in this study was identical to the mill-annealed material. It was vacuum heat-treated above the $\beta$-transus at 930 °C for 6 h and then furnace-cooled. It was then vacuum-annealed at 700 °C for 1 h and 40 min and air-cooled. Most colony sizes were between 100 and 200 $\mu$m. Preparation of $\beta$-annealed specimens included etching of the specimen surface prior to crack initiation. Etching revealed the microstructure of the specimen and enabled evaluation of the influence of each large grain on surface deformation orientation and shape.

Flat, Ti-6Al-4V dogbone samples were used in this study (Figure 2). Through electrodischarge machining, a 0.4 mm long notch was cut into the edge of the centre of the reduced section of each specimen to provide a stress concentration for crack initiation. All specimens were polished to a low surface roughness (root mean square $\approx$ 250 nm) prior to testing to provide a uniform surface finish and enable detailed examination of changes in surface topography.

Fatigue cracks were initiated from the notch of each specimen by high cycle fatigue loading. The specimens were subjected to low stress (*c.* 25% of yield stress) cyclic loading at a stress ratio of 0.1. In

 

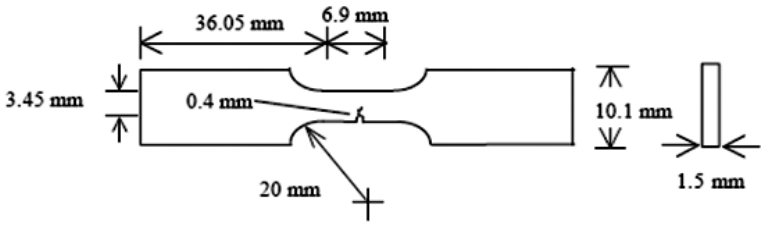


**Figure 2:** Specimen dimensions

order to initiate a short crack, 10 000 cycles were run during each set. Following each set of cycles, the specimen surface was examined with a travelling optical microscope. Once a visible crack was detected, the stress was reduced by 10% and the specimen was subjected to additional sets of 1000 cycles. Prior to each additional set, the stress was reduced by another 10%. This stress reduction was repeated several times to sharpen the crack front and reduce the initial surface deformation area (see Equation 1). The crack length ranged from 0.05 to 0.25 $\mu$m. Including the notch, effective crack length ranged from 0.45 to 0.8 $\mu$m.

Following crack initiation, the specimens were loaded into a portable static 4.5 kN load frame. The load frame was placed under a white-light interference profilometer for *in situ* topographical data acquisition in both cases, mill-annealed and $\beta$-annealed titanium alloys.

## Results and Discussion

The crack-tip deformation zone size of fatigue-pre-cracked material was monitored under increasing load until failure. The extent of deformation was

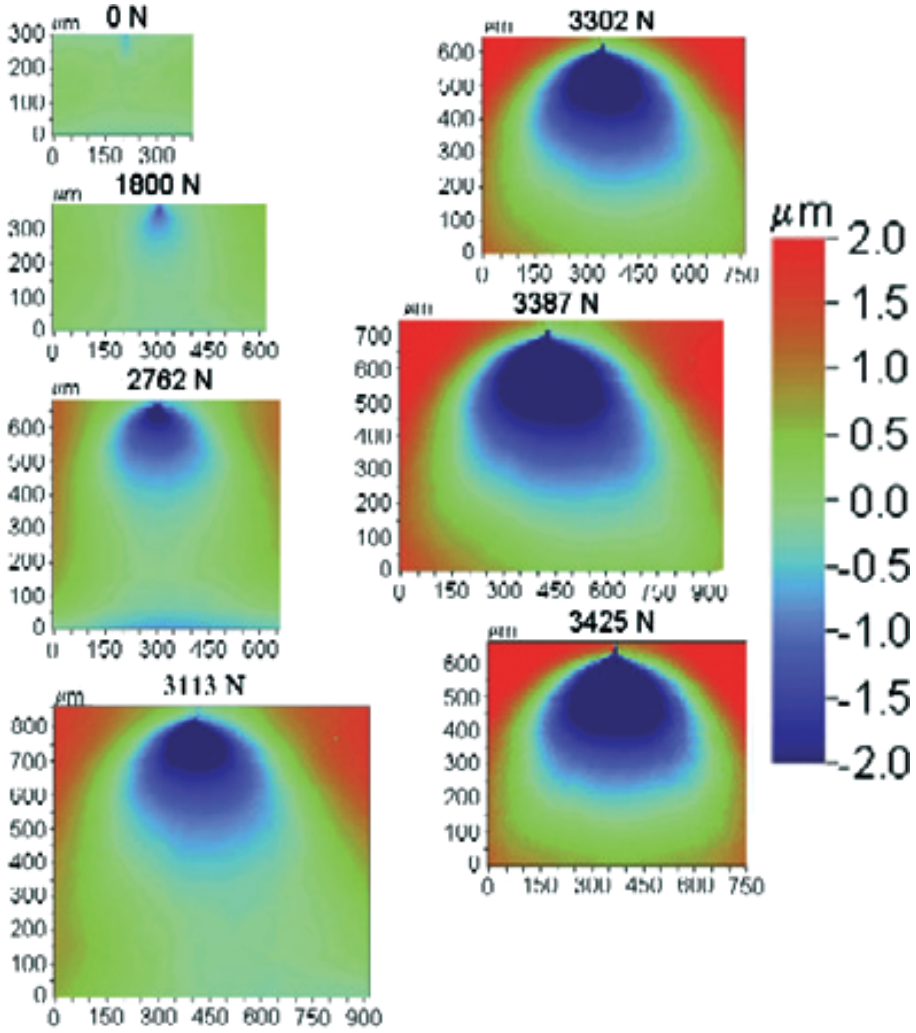


**Figure 3:** Profilometry images of accumulating deformation in a mill-annealed specimen

  

quantified using threshold calculations of surface-profiling data acquired by white-light interference microscopy. The threshold method is based on setting a numerical cutoff between the areas of depression and the gradual slope of the material into the background. All pixel points representing regions lower than the threshold value are summed for an area calculation. A value of zero, which corresponds to the height of the bulk sample, is the cutoff for area calculations used for evaluation of the data.

Profilometry images for mill-annealed and $\beta$-annealed materials, obtained under static load at incrementally increased levels, are shown in Figures 3 and 4, respectively. The presence of a distinct region of deformation ahead of the crack is observed in Figure 3. However, the deformation in $\beta$-annealed specimens (Figure 4) is uneven and varies from specimen to specimen as expected for a very coarse-grained material. The general shape of the deformation remains the same from the beginning of loading to development of crack instability. The deformation continues to accumulate as the magnitude of the load is increased. The symmetrical shape shown in Figure 3 is typical of relatively fine-grained materials like the mill-annealed microstructure used in this study. Coarse-grained or highly textured materials like the $\beta$-annealed microstructure develop a less symmetric plastic zone because the plastic deformation slip activity ahead of the crack tends to follow large grains oriented for easier slip or a preferred crystallographic orientation (Figure 4). Comparing Figures 3 and 4 clearly illustrates the dependence of deformation shape on the microstructure of the material.

Figure 5 shows optical images of cracks in both mill-annealed and $\beta$-annealed material prior to static

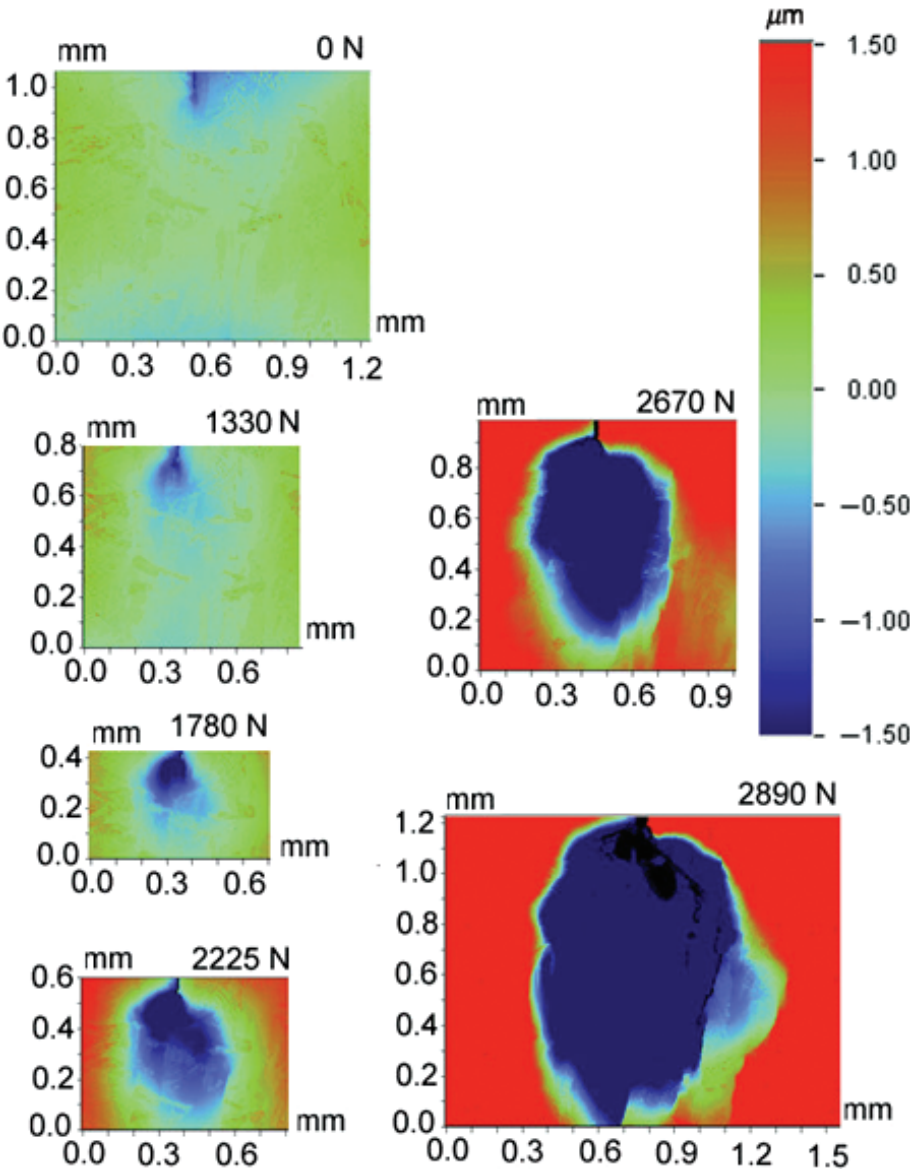


**Figure 4:** Profilometry images of accumulating deformation in a $\beta$-annealed specimen

loading and after release of a near-critical load. The deformation zone of the mill-annealed material is contained within the area marked by residual shear bands (Figure 5B). The deformation zone of the $\beta$-annealed material extends beyond the crack-tip opening (compare Figures 5D and 4). The crack front of the $\beta$-annealed material is more jagged because it follows the grains of the coarse microstructure. The area ahead of the crack front in the $\beta$-annealed material contains several small cracks that were created by crack branching. In addition, the crack length of both materials remained constant throughout loading until the point of unstable crack growth (Figure 5B,D).

A correlation between the observed surface deformation and plastic deformation is necessary to relate this work with accepted fracture mechanics laws. A rough comparison of theoretical plastic deformation and surface deformation was created by plotting the theoretical radius of plastic deformation for a *K*-level equivalent to that documented for a surface deformation image. The theoretical equation plotted (Equation 2) describes the radius of plastic deformation of a material in the plane stress condition and is based on an in-plane 2-D model. This equation is valid as the samples used in this study are thin enough for the plane stress condition to exist throughout their entire cross-section, but is only a

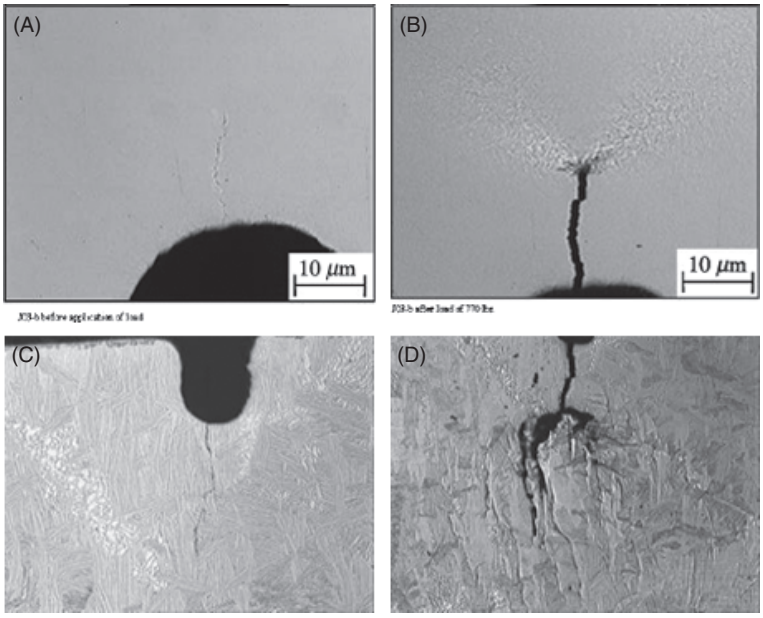


**Figure 5:** Optical images of deformation near crack tip. Mill-annealed material (A) prior to loading and (B) after unloading from 3425 N. $\beta$-annealed material (C) prior to loading and (D) following unloading of 2890 N

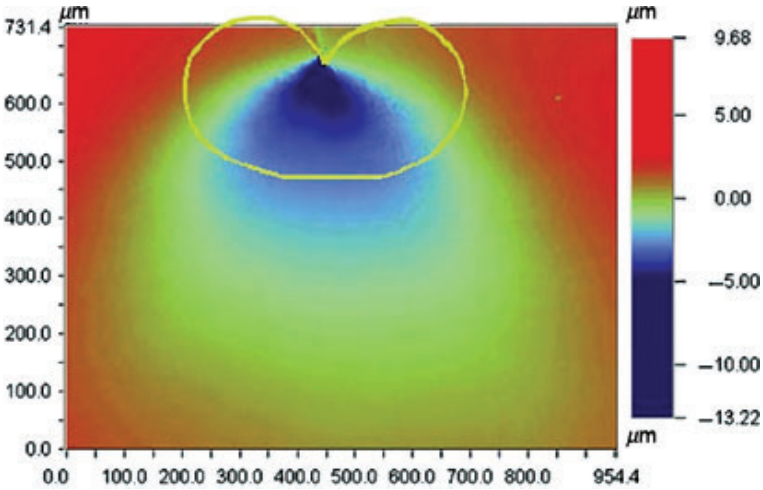


**Figure 6:** Theoretical plastic zone compared to surface deformation of mill-annealed material at 3114 N load

broad comparison as the surface deformations represent out-of-plane displacement or displacement perpendicular to the theoretical modelling plane. The theoretical radius was calculated, plotted as a function of $\theta$, and then sized to correlate with the figure over which it was overlaid. The theoretical plastic deformation shape did not represent the surface deformation (Figure 6). The difference in shape was justified because the kidney shape represents the in-plane material behaviour and the shape seen on the surface is the result of out-of-plane displacement.

The discrepancy in size may also result from the inclusion of both elastic and plastic contributions to the surface deformation. If these contributions were separated, one may discover that only the deepest area of deformation is representative of plastic deformation. With such consideration, the theoretical plastic zone size may more closely represent the experimental plastic zone size.

Based on fracture mechanics considerations, it is assumed that the deformation zone size would rapidly increase when the applied load developed to stress intensity levels, $K$, close to the critical stress intensity factor. The critical stress intensity factor for plane stress, $K_Q$, is referred to here instead of the critical stress intensity factor for plane strain, $K_{IC}$, because the stress state is dependent on the thickness of the thin samples used in this study. When the $K$-level in the cracked component reached the $K_Q$ value, fast fracture developed. The $K_Q$ values were easily obtained from valid plain stress fracture toughness tests. When the $K_Q$ value was reached it was impossible to stop or slow the failure. For this reason, the surface area of the deformation and volume of the depression zone, as determined by the surface profiling data, were plotted against the stress intensity factor. A relationship resulted from trends in the changes of surface deformation during the approach to $K_Q$.

Quantified data from the incrementally increased static load tests are shown in Figure 7. Area and volume data were calculated through analysis of images contained in Figures 3 and 4. The region of deformation ahead of the crack increased exponentially both in area and volume with the increasing stress intensity factor. Directly prior to failure, the area of deformation retracts (Figure 7A). Unlike area, the deformation volume continually increases with K until the final failure (Figure 7B). Data analysis indicates an exponential increase in the slope of the deformation volume versus stress intensity factor that indicates an upcoming plastic instability. Detection of this sudden increase in the slope of deformation volume over stress intensity factor may become a useful tool in anticipating eventual instability and may be a basis for methods to detect the beginning of fast fracture in structural components with sharp notches or existing cracks.

The surface deformation investigated throughout this work includes both plastic and elastic contributions. A substantial amount of the elastic

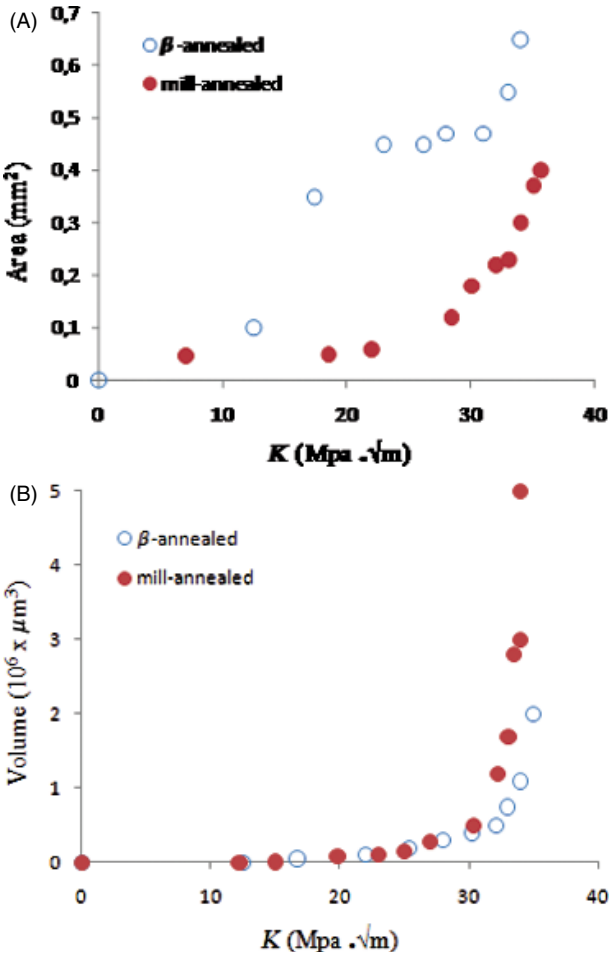


**Figure 7:** Deformation and stress factor relationship of Ti-6Al-4V for (A) area of deformation and (B) volume of depression for $\beta$-annealed and mill-annealed microstructures

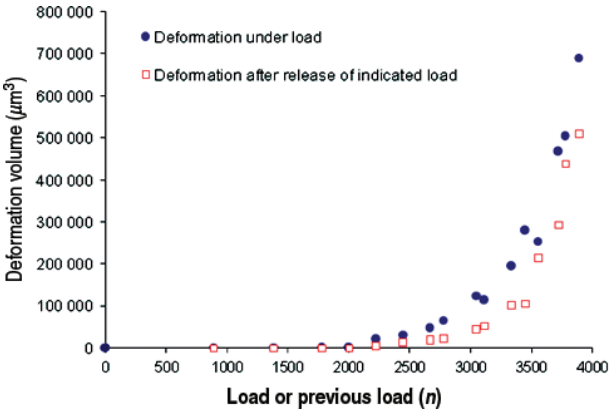


**Figure 8:** Deformation relaxation after release of load for mill-annealed material

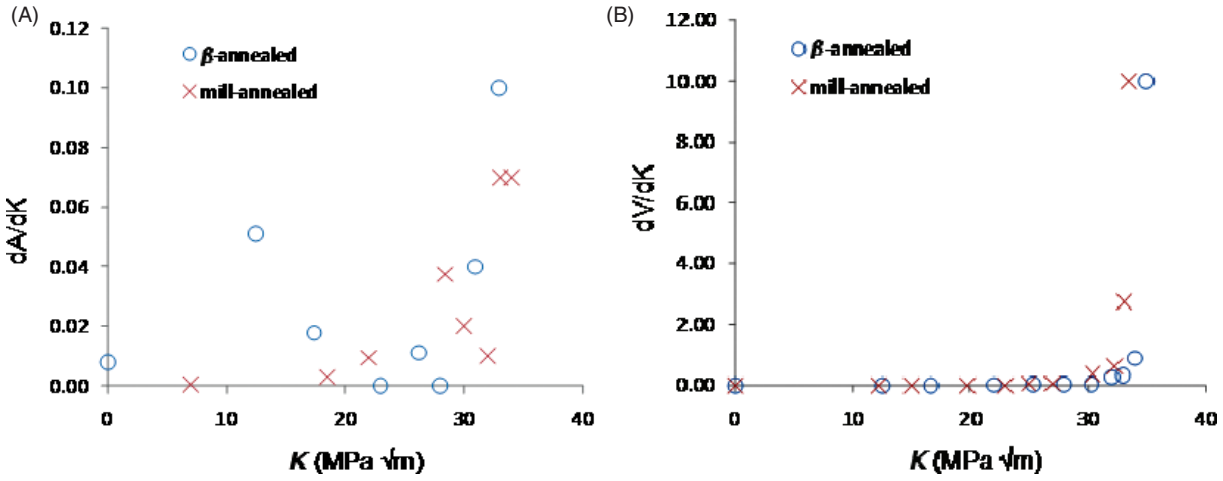


**Figure 9:** Rate of change in Deformation vs. stress intensity factor for Ti-6Al-4V for (A) area of deformation and (B) volume of depression, for $\beta$-annealed and mill-annealed microstructures

deformation was expected to relax upon release of the static load. To track this deformation retraction, images of the specimen were taken under load and then directly following release of the load. Measurements showed a minimal decrease in the deformation area. This strain release was time-dependent and could be traced over a period of several hours. An additional study was performed to determine if the relative amount of elastic to plastic deformation decreased as deformation size increased. The relationship between elastic and plastic deformation was tracked by loading a specimen to a specific load, imaging the sample under load, releasing the load and immediately imaging the sample without load. The result of this test is presented in Figure 8. The duration of time the sample was under load was relatively constant for all load steps. The percentage of relaxed deformation was calculated at each load step using Equation (3).

$$\%\ \text{of relaxed deformation} = \frac{\text{Deformation under load} - \text{Deformation with no load}}{\text{Deformation with no load}} \times 100 \quad (3)$$

At loads up to half the critical load of the sample, just over 20% of the deformation relaxed upon release of the load. At loads over half of the critical load, 60% of the deformation relaxed. Most importantly, after deformation relaxation the exponential relationship between the deformation size and the stress intensity factor remained.

Examination of the common relationship between deformation zone size and the stress intensity factor indicates that criteria for failure may be extracted from surface deformation data. The suggested criterion for failure is a critical rate of change of depression volume, $r_c = dV/dK$, at a determined point prior to failure. This criterion is further supported by Figure 9A,B. Figure 9A shows the rate of change in area of deformation versus the stress intensity factor for Ti-6Al-4V material with $\beta$-annealed and mill-annealed microstructures. Based on this plot, a critical value of $K$, where rapid change occurs in the area of deformation, cannot be clearly defined. This is attributed to the fact that the area of deformation retracts directly prior to failure (Figure 7A). However, the deformation volume continually increases with $K$ until the final failure (Figure 7B). As a result, a critical rate of change in the volume of depression, which corresponds to the slope of the size of deformation over the stress intensity factor at a determined point prior to failure, can be easily determined (Figure 9B). Based on this analysis, the critical stress intensity factor for plane stress, $K_Q$, was determined for Ti-6Al-4V specimens: $K_Q$ = 33.5 MPa √m for $\beta$-annealed microstructure, and $K_Q$ = 32.8 MPa √m for mill-annealed microstructure.

## Conclusion

Profiling measurements using white-light interference microscopy quantified the surface area, volume and shape of the deformation zone ahead of the crack tip of fatigue pre-cracked titanium alloy specimens subjected to static loading. An exponential

  

relationship between the surface area and volume of the deformation zone and the stress intensity factor of the cracked sample was obtained. This relationship was found to be common to different microstructural conditions, such as mill-annealed and $\beta$-annealed microstructures. These observations enabled the determination of a critical rate of change in volume of depression at a crack tip versus the stress intensity factor that can be used to predict catastrophic failure of the material. As a result, the critical stress intensity factor for plane stress, $K_Q$, was determined for Ti-6Al-4V specimens with both $\beta$-annealed and mill-annealed microstructures. Additional observations include time-dependent crack-tip depression zone enlargement under sustained load, crack-tip deformation relaxation following load release and discrepancies between surface deformation and theoretical plastic deformation shapes. The outcome of this study can have important implications for optimising the service life of airframe structural components.

## ACKNOWLEDGEMENTS

The contribution of J. Schroeder and Prof. D. Eylon to this study is specially acknowledged.

## REFERENCES

1. Finney, J. M. (1994) *Fatigue Crack Growth in Metallic Military Aircraft Structures*, Handbook of Fatigue Crack Propagation in Metallic Structures, Vol. 2, Elsevier Science B.V., Amsterdam, NL, pp. 1539–1541.
2. Schroeder, J., Shell, E. B., Matikas, T. E. and Eylon, D. (1999) Development of methods to observe fatigue damage through surface characteristics. *Proc. SPIE Conf. Nondestructive Eval. Aging Mater. Composites III*, vol. 3585, Newport Beach, CA, USA. pp. 117–124.
3. Schroeder, J., Matikas, T. E. and Eylon, D. (1998) *Development of methods to observe material's fatigue damage through surface characteristics*. DARPA/AFOSR MURI Second Annual Report, pp. A5-1 to A5-13, August 1998.
4. Schroeder, J., Matikas, T. E. and Eylon, D. (1999) *Evaluation of a proposed methodology to Predict Fatigue Crack Instability in Aerospace Alloys*. DARPA/AFOSR MURI Third Annual Report, UDR-TR-1999-00073, p. 16, September 1999.
5. Boyer, R. R. (1996) An overview on the use of titanium in the aerospace industry. *Mater. Sci. Eng.* **A213**, 103–114.
6. Schroeder, J., Eylon, D., Shell, E. B. and Matikas, T. E. (2000) Development of Nondestructive Method for Prediction of Crack Instability. In *Nondestructive Methods for Materials Characterization*, Vol. 591 (G. Y. Baaklini, N. Meyendorf, T. E. Matikas and R. S. Gilmore, Eds). MRS Publication, Warrendale, PA: pp. 61–66.
7. Harmain, G. A. and Provan, J. W. (1997) Fatigue crack-tip plasticity revisited – the issue of shape addressed. *Theor. Appl. Fracture Mech.* **26**, 63–79.
8. Sih, G. C. (1973) Some basic problems in fracture mechanics and new concepts. *Eng. Fracture Mech.* **5**, 365–377.
9. Barker, D. B., Sanford, R. J. and Chona, R. (1985) Determining K and related stress-field parameters from displacement fields. *Exp. Mech.* **25**, 399–407.
10. Sanford, R. J. and Daily, J. W. (1979) A general method for determining mixedmode stress intensity factors from isochromatic fringe patterns. *Eng. Fract. Mech.* **11**, 621–633.
11. Kang, B. S. J., Zhuang, Y. N. and Liu, Q. K. (1992) Experimental investigation of creep-crack-tip deformation using moiré interferometry. *Exp. Mech.* **32**, 309–315.
12. Nishioka, T., Yao, J., Sakakura, K. and Epstein, J. S. (2000) Measurements of near-tip displacement fields, separated J integrals and separated energy release rates for interfacial cracks using phase-shifting moiré interferometry. *JSME Int. J. Ser. A* **43**, 334–342.
13. Krishnamoorthy, H. and Tippur, H. V. (1999) Extracting fracture parameters using local collocation of full-field displacement data. *Exp. Tech.* **22**, 22–25.
14. Dadkhah, M. S., Kobayashi, A. S., Wang, F. X. and Grasser, D. L. (1988) J-Integral measurement using moiré interferometry. *Proc. VI Int. Cong. Exp. Mech.* Portland, OR, 227–234.
15. Bastawros, A. F. and Kim, K. S. (2000) Experimental analysis of nearcrack-tip plastic flow and deformation characteristics (I): polycrystalline aluminum. *J. Mech. Phys. Solids*, **48**, 67–98.
16. Nishizawa, H. and Ogawa, T. (2005) Mode II fatigue crack growth characteristics and experimental evaluation of the crack driving force. *Zairyo/J. Soc. Mater. Sci.* **54**, 1295–1300.
17. Dudderar, T. D. and Gorman, H. J. (1973) The determination of mode I stress intensity factors by holographic interferometry. *Exp. Mech.* **13**, 145–149.
18. Ramaswamy, S., Tippur, H. V. and Xu, L. (1993) Mixed-mode crack-tip deformations studied using modified flexural specimen and coherent gradient sensing. *Exp. Mech.* **33**, 218–227.
19. Han, G., Sutton, M. A. and Chao, Y. J. (1994) A study of stationary crack-tip deformation fields in this sheets by computer vision. *Exp. Mech.* **34**, 125–140.
20. Shih, C. F., Andrews, W. R. and Delorenxi, R. G. (1974) Studies on crack initiation and stable crack growth. In: *Elastic-Plastic Fracture* (J. D. Lands, J. A. Begley and G. A. Clarke, Eds). ASTM STP 668, Amer. Soc. Test. Mat., Philadelphia, PA: pp. 170–186.
21. Yoneyama, S., Kobayashi, Y. and Ogawa, T. (2006) A method for evaluating mixed-mode stress intensity factors from displacement fields around a crack tip. Nihon Kikai Gakkai Ronbunshu, A Hen. *Trans. Japan Soc. Mech. Eng. A* **72**, 1025–1032.
22. Yoneyama, S., Ogawa, T. and Kobayashi, Y. (2007) Evaluating mixed-mode stress intensity factors from full-field displacement fields obtained by optical methods. *Eng. Fract. Mech.* **74**, 1399–1412.
23. Sanford, R. J. (1989) Determining fracture parameters with full-field optical methods. *Exp. Mech.* **29**, 241–247.

 

24. Schroeder, J. (2000) *Use of White Light Interference Profilometry to Develop a Nondestructive Method to Predict Instability of Loaded Cracks*. M.S. Thesis, University of Dayton, OH, May 2000.

25. Caber, P. (1997) Interferometer characterizes laser-textured steel. *Laser Focus World* **33**, 157–158.

26. Bowe, B. and Toal, V. (1998) White light interferometric surface profiler. *Optical Eng.* **37**, 1796–1799.

27. Raz, E. (1996) A multiple white light interferometer. *Rev. Sci. Instrum.* **67**, 3416–3419.

  